Capturing the Random Changes in Process Parameters in the Stochastic Grey-box Model of the Flow-Front Dynamics

Relan, Rishi; Nauheimer, Michael; Madsen, Henrik

Published in:
IFAC-PapersOnLine

Link to article, DOI:
10.1016/j.ifacol.2019.10.015

Publication date:
2019

Document Version
Publisher's PDF, also known as Version of record

Available online at www.sciencedirect.com

ScienceDirect

IFAC PapersOnline CONFERENCE PAPER ARCHIVE

IFAC PapersOnLine 52-10 (2019) 31–36

Capturing the Random Changes in Process Parameters in the Stochastic Grey-box Model of the Flow-Front Dynamics

Rishi Relan * **Michael Nauheimer** ** **Henrik Madsen** *

* *DTU Compute, Technical University of Denmark, Denmark (e-mail: risre@dtu.dk, hmad@dtu.dk)*

** *Siemens Gamesa Renewable Energy, Denmark (e-mail: michael.nauheimer@siemensgamesa.com)*

Abstract: With the continuously increasing size of the wind turbine blades, the complexity of the casting process and the risk of failures has also increased. The *IntegralBlades*® vacuum assisted resin transfer moulding (VATRM) production process at the *Siemens Gamesa Renewable Energy* facility in Aalborg, Denmark, does not permit the visual inspection of the process. Hence a sensor system (possibly virtual) for process control and monitoring is highly prized. Furthermore, the effect of material handling, variations in permeability of the casting media and the material (epoxy) properties affect the outcome of the casting process. Therefore, it is necessary to analyse the effect of such variations at an early stage of the design process (e.g. during the simulations) of such a sensor system. Therefore, in this paper, we first describe an effective method to simulate the random changes in the permeability and viscosity in high-dimensional partial differential equations based model of the fluid flow. Next, a low-dimensional grey-box (cyber-physical) spatiotemporal model is proposed to capture the effect of random change in permeability and viscosity during the progression of the flow-front. Finally, a numerical case-study is presented demonstrating the effectiveness of the proposed methodology.

Keywords: Wind turbines, Partial differential equations, Numerical simulations, Stochastic differential equations, Grey-box modelling, Maximum likelihood estimation.

1. INTRODUCTION

The vacuum assisted resin transfer moulding (VARTM) process is commonly used to manufacture large-scale composite shell structures like wind turbine blades. The VARTM process generally involves infusing a thermoset polymer like epoxy resin into a glass fibre reinforced preform mould through several inlets. The pressure difference between the mould and the ambient pressure of one bar in the production area drives the progression of the epoxy resin inside the mould. Heterogeneous nature of the fluid flow inside the mould increases the risk of defects such as dry spots and voids, leading to the deterioration of the mechanical structure (Park et al., 2011; Matuzaki et al., 2015). Hence, for better fault diagnosis, prognosis and control of the process, it is vital to continuously monitor the evolution of the flow-front in real-time inside the mould in a VARTM process.

Various modalities of the sensors like the optical fibres (Kueh et al., 2002), permittivity sensors (Yenilmez and Sozer, 2009), pressure sensors (Zhang et al., 2011), and sensors based on electrical time-domain reflectometry (Dominauskas et al., 2003; Buchmann et al., 2016) have been reported in the literature to monitor the VARTM processes. The drawback for most of these sensors is that they are limited to measuring on or close to the surface of the moulded parts.

Inspection of the infusion process is commonly done by visually observing the process. By using the knowledge from visual observations it is possible for the production workers to take action to ensure proper impregnation of the materials in the moulds. In a recent study, (Matsuzaki and Shiota, 2016) proposed a method to use the two-sided visual observations for 4-dimensional data assimilation to accurately reconstruct the 3-dimensional resin flow and permeability filed of a fibre preform. However, the wind turbine blades produced at the *Siemens Gamesa Renewable Energy* production facility in Aalborg, Denmark, are cast in one piece using the patented *IntegralBlades*® technology (Stiesdal et al., 2006) instead of two separate half blades which are then united afterwards. Hence, in this technology, real-time visual inspection of the casting process is not possible. Thus, research engineers at *Siemens Gamesa Renewable Energy* are looking to develop an automated flow-front monitoring system to control the process of mould filling. Real-time control of the trajectory of the flow-front inside the mould decreases the potential risk of dry spots, thereby also reducing the repair time and increasing the general structural quality of the produced blade.

In (Nauheimer et al., 2018b) proposed a coupled stochastic differential equations (SDEs) based spatiotemporal model

⋆ We thank the *Manufacturing Academy of Denmark* (MADE) for providing the financial support. We thank the laboratory employees at *Siemens Gamesa Renewable Energy* for their co-operation.

10.1016/j.ifacol.2019.10.015

to estimate the dynamics of the flow-front inside the mould. For the validation of the model, different datasets (patterns) of the flow-front evolution inside the mould were simulated using the partial differential equations (PDEs) but did not account for the change in process parameters such as the permeability and the viscosity.

For example, the permeability of a glass fibre preform can vary due to the handling of glass fibre mats (pulling/stretching, stacking etc. Similarly, the viscosity of the epoxy is another source of uncertainty in the process of casting a wind turbine blade. The viscosity of epoxy is dependent on temperature and time. An increase in the temperature will result in low viscosity. However, as soon as the epoxy and the hardener are mixed, an irreversible curing process starts. Epoxy cures continuously over time which results in a continuous increase of the viscosity. This process results in the viscosity of the epoxy being dependent on the cure degree. Furthermore, an increase of the temperature results in an increasing cure rate.

The change in material property and process parameters may result in a heterogeneous progression of the resin flow-front. A heterogeneous flow-front can cause improper impregnation of the fibre preform that requires repair of the final blade. The repair of the blades is a time-consuming process. Furthermore, the repair may jeopardise the structural integrity of the blades. In a worst-case scenario, the final blade may have to be discarded.

Hence, it is crucial to account for changes in process parameters at an early stage of the design stage, e.g. the simulation phase. A first attempt to include the change in permeability as a point change and a linear change in viscosity during the finite element simulation of the PDEs model of the flow-front evolution is reported in (Nauheimer et al. (2018a)). This approach does not reflect the actual change in permeability of the media during the casting process because pulling/stretching of the media can also change the permeability spatially around local cells. Furthermore, the authors did not account for such changes in permeability and viscosity in the SDEs based model. Therefore, in this paper, we improve the PDE based model to include the spatial variation in permeability and a linear increase in viscosity. Furthermore, we extend the coupled SDEs based grey-box model structure of the flow-front to account for such changes.

The paper is structured as follows: Section 2 briefly describes the VARTM process, and the PDE based formulation of the problem is discussed in Section 2.1. In Section 3, the finite element method based numerical simulation details of the PDE model are discussed. A coupled SDEs based grey-box model for estimation of the flow-front including the effect of the change in process parameters is proposed in Section 4. Section 5 describes the results and finally the conclusions are given in Section 6.

2. THE VARTM PROCESS

In the VARTM process, a glass fibre casting mould is infused with liquid epoxy. The process is only governed by the pressure difference between the inside of the mould, i.e. ≈ 0 bar and the ambient pressure of ≈ 1 bar (see Fig. 1). The pressure gradient, permeability, porosity of the

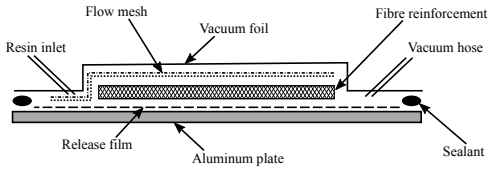

Fig. 1. The resin enters through the resin inlet into the vacuum bag and spreads (from left to right) into the pores of the fibre reinforcement. To assist this process, a vacuum is generated through the vacuum hose.

auxiliary materials inside the mould along with the effect of the local temperatures on the viscosity of the epoxy mainly determines the direction and the velocity of the flow inside the mould.

2.1 Mathematical Formulation of Flow in a Porous Medium

The flow of epoxy inside a rectangular mould can be described using partial differential equations (PDEs). For modelling the spatiotemporal evolution of the flow-front along the y direction, it is assumed that flow along the line sensors can be measured (see dotted lines along the y-direction in Fig. 2).

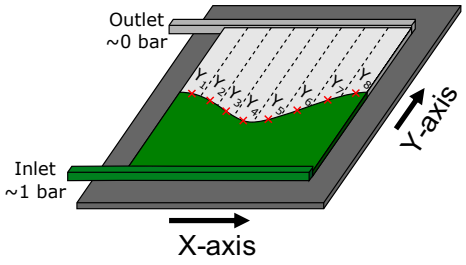

Fig. 2. The line sensors (dotted lines) are placed equidistantly to split the x-direction into cells. The red crosses along the y-direction represent the points where the line sensors measure the flow.

***Assumption** 2.1.* The Darcy's law based 2-D (spatial dimensions) PDE model is a good approximation of the physics of the flow in three spatial dimensions.

***Remark** 2.1.* The 2-dimensional formulation is a reasonably good approximation because the thickness of the laminate is generally much smaller than the other two dimensions. However, the case study can be extended to 3-dimensional formulation.

The volumetric flow velocity $\mathbf{q} = \mathbf{q}(x, y, z, t)$ [m^3/s] of a fluid in a porous medium in three dimensions is described by the *Darcy's law* (Darcy, 1856). Under the assumption that a two (spatial) dimensional PDE model based on *Darcy's law* provides a good description of the physics of the flow in three (spatial) dimensions, here we formulate an in-plane flow model only in two spatial dimensions,

$$\mathbf{q} = -\frac{\boldsymbol{\kappa}\varphi H}{\mu}\nabla p \tag{1}$$

where $\mathbf{q} = \mathbf{q}(x, y, t)$ represents the flow velocity integrated along the vertical axis in [m/s], $\boldsymbol{\kappa} = \boldsymbol{\kappa}(x, y)$ represents the permeability tensor for the porous medium in [m^2], φ is the porosity of the medium [-], H is the cross-sectional thickness [m], the fluid viscosity is given by $\mu = \mu(x, y, t)$

[Pa·s], $p = p(x, y, t)$ is the pressure [Pa], and the in-plane spatial derivative [1/m] is given by $\nabla = (\frac{\partial}{\partial_x}, \frac{\partial}{\partial_y})$. Combining this with the conservation of mass results in

$$\dot{h} + \nabla \cdot \mathbf{q} = 0 \tag{2}$$

where the thickness of the fluid layer is given by $h = h(x, y, t) \leq H$. By assuming the following relationship

$$h = \min\left(\varphi H, \frac{p}{\rho g}\right) \tag{3}$$

where g is the gravitational force, and ρ is the density of the fluid. Equation (3) corresponds to local hydrostatic equilibrium. This condition implies that the pressure is proportional to the thickness of the fluid layer where the gap is partially filled with epoxy, but it may be larger when the gap is completely filled with epoxy. By combining equations (2) and (3) we can now eliminate h from the model formulation to obtain:

$$\dot{h} = \frac{\mathrm{d}h}{\mathrm{d}p}\dot{p} = \nabla \cdot \left(\frac{\boldsymbol{\kappa}\varphi H}{\mu}\nabla p\right) \tag{4}$$

Finally, we complete the PDE governing p with boundary conditions by assuming no-flux boundary conditions along the sides, a pressure of $p_0 = 1$ bar at the inlet, and a pressure of zero bar at the outlet of the casting respectively.

3. GENERATING THE FLOW-FRONT DATA

The open-source numerical PDE solver *FEniCS* is used to solve and generate the flow-front evolution data (Alnæs et al., 2015). To discretize space the *FEniCS* solver employs the finite element method. For this case-study, we solve the PDE described in (4) for a $L_x \times L_y$ (80 cm × 90 cm) rectangular system similar to the one shown in Fig. 2. . This is equivalent to numerically solving a system of $(n_x + 1) \times (n_y + 1)$ (i.e. 65×129) vertices.

3.1 Heterogeneous Evolution of the Flow-Front

Generally homogeneity of the flow-front during the infusion process is ensured during the placement of glass fibre and auxiliary materials inside a blade mould. However, sometimes during the infusion process, manufacturing process errors result in perturbations that affect the flow-front progression. Therefore, we consider here the heterogeneous case. In the case of a heterogeneous evolution of the flow-front, $\frac{\kappa}{\mu}$ is kept constant w.r.t. the time but along the spatial directions the model is described as

$$\frac{\kappa}{\mu} = \frac{c_0}{\left(1 - A \cdot \cos\left(\frac{2\pi x}{L_x}\right)\right)\left(1 - A \cdot \cos\left(\frac{2\pi y}{L_y}\right)\right)} \tag{5}$$

where the constant A determines the relative decrease in permeability towards the middle of the casting, c_0 is a correction constant. This model simulates a reduction in the permeability towards the centre of the casting. Similarly, any nonlinear function can be used to simulate the change in permeability along the spatial domain.

3.2 Capturing Parameters Variations

As discussed earlier, the permeability of the glass fibre preform and viscosity of the epoxy can change randomly during operating conditions. Therefore in this Section, we explain briefly how these variations can be included while numerically simulating the above formulated PDEs to generate a realistic dataset for the flow-front evolution.

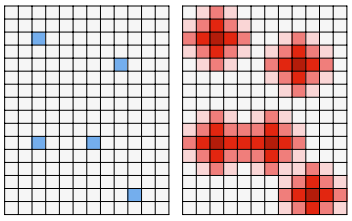

Fig. 3. Shows a visual representation of the convolution described in (6)

Modelling the random change in permeability: To numerically simulate the change in permeability, first, we randomly select the cells around which the variations in permeability occurs as in (Nauheimer et al., 2018a). As mentioned before, when a glass fibre mat is stretched it will change the porosity and permeability across an entire area; therefore the proposed approach in (Nauheimer et al., 2018a) may not reflect the reality. Hence, to simulate how the permeability is distributed around the chosen random cell, we define a matrix, $D \in \mathbb{R}^{p \times q}$. The matrix D is then to be convoluted, in two dimensions, with a matrix, $M_R \in \mathbb{R}^{O \times V}$, describing around which randomly chosen cells the permeability varies. This operation can be defined by a two-dimensional convolution as

$$(M_R * D)(|, \|) = \sum_o \sum_v M_R(o, v) D(j - o + 1, k - v + 1) \tag{6}$$

To have a semi-symmetrical distribution of the permeability variation around the chosen random cells given in M_R, the values P and Q, describing the size of D, both have to be odd numbers smaller than O and V, respectively. All values of D, where one or both of the indices $j - o + 1$ or $k - v + 1$ are not within the size of D (1,...,O, 1,...,V), are treated as zero (zero padding). The result of this convolution is a matrix of size $(o + p - 1) \times (v + q - 1)$. The central part of the resulting matrix has the same size as M_R. Fig. 3 shows a visual representation of the convolution described in (6).

Modelling change in viscosity: The temperature of the mould is generally kept constant during the infusion. However, local variations in the temperature might occur due to external temperature variations. The local temperature usually is not measured, and this adds uncertainty when estimating the viscosity. It is, however, fair to assume that locally the temperature only has minor variations w.r.t the neighbouring cells. This effect can be described similarly to the random permeability term defined in (6). However, contrary to the permeability, the temperature and thereby the viscosity in each cell can vary w.r.t. time. This can be defined as

$$\mu(t) = \mu_0(t) + \mu_1(t) \tag{7}$$

where μ_0 is the initial viscosity and μ_1 is the viscosity change rate.

3.3 Numerical Simulations

For obtaining a numerical solution to the formulated PDEs, a semi-implicit Euler solver is used to time-march.

The derivative $\dot{p}$ is approximated by a first-order finite difference and the evaluation of the derivative $\frac{dh}{dp}$ is done at the previous time step. Furthermore, the right-hand side of (4) is solved at the next time step. Since the derivative $\frac{dh}{dp}$ is zero in those parts of the spatial domain that have already been filled with the fluid; therefore the problem can be considered as differential-algebraic. The simulated flow-front progression data $\mathcal{Z}_{l,t}$ for each line, $l = 1, ..., n_x + 1$, is generated by evaluating only those $n_y + 1$ vertices along the y-axis where the pressure greater than the threshold, p_{TH}, for all n_x+1 vertices spread across the x-axis of the considered system.

$$\mathcal{Z}_{i,t} = \frac{\sum_{\mathbb{K}=1}^{n_y+1} \max(\min(p(x_n, y_{\mathbb{K}}, t), p_{\mathrm{TH}}), 0)}{p_{\mathrm{TH}} \cdot (n_y + 1)} L_y \tag{8}$$

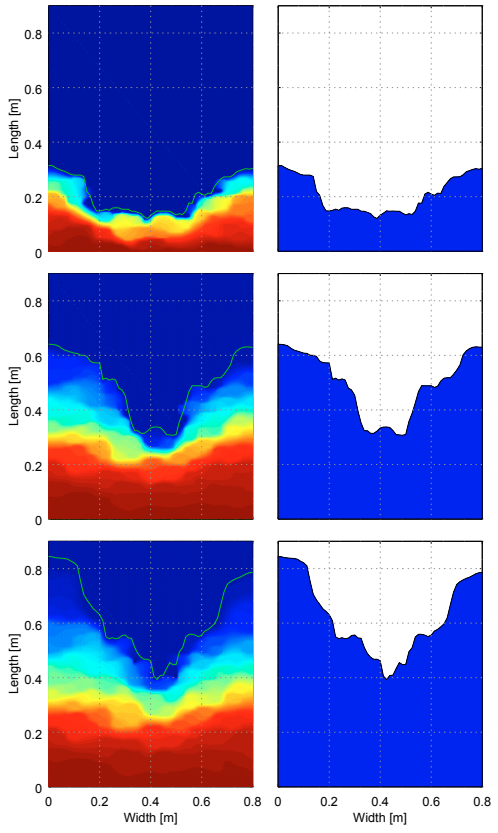

Fig. 4. The plots in the left column show a contour plot of the pressure distribution. The red colour indicates a high pressure of 1 bar; the blue colour indicates a low pressure of 0 bar and the green line represents the boundary of the generated flow-front data. The right column show the evolution of the generated flow-front data corresponding to the green line.

Fig. 4 shows a heterogeneous flow-front progression with changes in permeability and viscosity. The three plots on the left column show the contour plot of the pressure distribution. The red colour indicates high pressure of 1 bar whereas the blue colour represents a low pressure of 0 bar. The green colour represents the simulated flow-front data. Three plots in the right column show the generated flow-front measurement data corresponding to the green line in the left column. A decrease flow rate towards the middle caused by a decrease in the permeability can also be observed in Fig. 4.

Even though the high-dimensional PDEs based model of the flow-front is useful to simulate the propagation of the flow-front inside the mould for different scenarios and operating conditions (e.g. permeability, temperature etc.) as demonstrated, the model is not very useful for real-time control and monitoring. Hence in the next section, a coupled stochastic differential equation (SDE) based grey-box modelling approach to model the flow-front dynamics is described (Øksendal, 2010).

4. GREY-BOX MODELLING

SDEs based grey-box models are based on a combination of physical knowledge (the structure of the model) of the system, as in the white-box models, and the statistical information based on the observed data like the black-box models (Kristensen et al., 2004a,b). The SDE formulation allows separating the time evolution of the states of a dynamical system into the drift term f_t and the diffusion term σ_t respectively. This explicit separation allows distinguishing between the modelling error due to unmodelled dynamics using the diffusion term and the measurement noise, resulting in an accurate description of the system dynamics. The drift and the diffusion terms can be described by a linear or a nonlinear function as described below (Øksendal, 2010)

$$\mathrm{d}Y_t = \underbrace{f_t(Y_t, U_t, t, \theta)\mathrm{d}t}_{\text{Drift}} + \underbrace{\sigma_t(Y_t, U_t, t, \theta)\mathrm{d}W_t}_{\text{Diffusion}}; \;\; t_0 \leq t \leq T, \tag{9}$$

where $t \in \mathbb{R}$ is the time and t_k, $k = 0, \cdots, N$ are the sampling time instants. The stochastic state equations with state variable $Y_t \in \mathcal{Y} \subset \mathbb{R}^n$ are formulated in continuous-time. The stochastic initial condition Y_{t_0} satisfies $\mathbb{E}[\|(Y_{t_0})\|^2] < \infty$ and vector of the system's deterministic inputs $U_t \in \mathbb{R}^d$ is known for all t. $W_t = (W_t^1, W_t^2, \cdots, W_t^m)^T \in \mathbb{R}^m$ is a standard Wiener process with an incremental covariance Q_t. For computational convenience, in this paper, the diffusion term is considered to be independent of the state variables i.e.

$$\mathrm{d}Y_t = \underbrace{f_t(Y_{t_k}, U_{t_k}, t_k, \theta)\mathrm{d}t}_{\text{Drift}} + \underbrace{\sigma_t(U_{t_k}, t_k, \theta)\mathrm{d}W_t}_{\text{Diffusion}}; \;\; t_0 \leq t \leq T, \tag{10}$$

The discrete-time measurements Z_{t_k} of the observable states are connected to the continuous-time state equation 9 through a nonlinear function $g_{t_k}(Y_k, U_k, t_k, \theta) \in \mathbb{R}^{\mathcal{L}}$ in the observation equation as shown below (11)

$$Z_{t_k} = g_{t_k}(Y_{t_k}, U_{t_k}, t_k, \theta) + \underbrace{e_{t_k}}_{\text{Measurement noise}} \tag{11}$$

$Z_{t_k} \in \mathcal{Z} \subset \mathbb{R}^{\mathcal{L}}$ is a vector of the system's outputs; $\theta \in \Theta \subset \mathbb{R}^p$ represents the vector of parameters of the system and e_{t_k} is a $\mathcal{L}$-dimensional zero mean Gaussian white noise process with covariance S_{t_k}.

4.1 Finite Difference Approximation of the Spatial Domain

The Darcy's Law described in (1) can be written to describe the flow-front progression along multiple one-

dimensional lines as shown in Fig. 2. The following relations hold for small values of H;

$$\frac{dY}{dt} = \frac{q(y,t)}{\varphi H} = -\frac{\kappa}{\mu} \cdot \nabla p, \tag{12}$$

$$p(x,y,t) = p_0 \cdot \max(0, 1 - \frac{y}{Y_t}), \tag{13}$$

then for each line i the flow can be desribed as

$$\frac{\mathrm{d}Y_{i,t}}{\mathrm{d}t} = \frac{\kappa p_0}{\mu}\frac{1}{Y_{i,t}}, \tag{14}$$

where under the assumption of perfect homogeneity of the flow-front $Y_{i,t}$ is the flow-front evolution in [m/s] along each line i where, $i = 1, ..., n$. The heterogeneous nature of multidimensional flow can be accommodated by introducing a spatial discretization term, $\mathcal{G}_{i,j}(Y_{i,t}, t)$ along the x-axis together with an active diffusion term $\sigma_{i,t}\mathrm{d}W_t$, to parameterize any differences between the model and the true system

$$\mathrm{d}Y_{i,t} = \left(\frac{C_{0,i}}{Y_{i,t}} + D_0\mathcal{G}_{i,j}(Y_{i,t}, t)\right)\mathrm{d}t + \sigma_{i,t}\mathrm{d}W_t \tag{15}$$

where D_0 represents the spatial coupling coefficient between two adjacent line sensors, $C_{0,i}$ is the value of $\frac{\kappa p_0}{\mu}$ for each line sensor. Except for the boundary cases ($i = 1, .., \frac{j}{2}$ or $i = n - \frac{j}{2} + 1, ..., n$) where the symmetric forward or backward finite difference approximations are used, the central finite difference approximations are used.

In (Nauheimer et al. (2018a)), the above model structure with a second-order $\mathcal{G}_{i,2}(Y_{i,t}, t)$ finite difference approximation of the spatial domain was fitted to the data generated by point-wise random perturbations of permeability and a linear increase in viscosity. The results indicated that perturbations caused especially due to the combined effect of a point change in permeability and a linearly (w.r.t. the time) increasing viscosity, decrease the precision of the estimated SDE model. Therefore in this study, we modify the model structure in (15) to include a separate permeability parameter κ_i for each line and one global viscosity term for all measurement lines. Furthermore to accommodate the effect of random spatial perturbations in permeability which can cause the spatial coupling parameters to be different between each set of measurement lines the SDE model structure is modified as follows

$$\mathrm{d}Y_{i,t} = \left(\frac{\kappa_i}{\mu_t}\frac{1}{Y_{i,t}} + \frac{\Lambda_{i,t}}{(\Delta x_m)^2}\right)\mathrm{d}t + \sigma_{i,t}\mathrm{d}W_t \tag{16}$$

$$\mathrm{d}\mu_t = \mu_c\mathrm{d}t + \mathrm{d}W_{\mu,t} \tag{17}$$

$$\mathrm{d}\kappa_{i,t} = \mathrm{d}w_{\kappa,i,t} \tag{18}$$

where $D_{(i,i-1),t} = D_{(i-1,i),t}$ and $\Lambda_{i,t} = D_{(i-1,i),t}(Y_{i-1,t} - Y_{i,t}) + D_{(i+1,i),t}(Y_{i+1,t} - Y_{i,t})$. In the next Section, the parameter estimation problem of this grey-box model structure is formulated as the maximum likelihood estimation problem.

4.2 Maximum Likelihood Estimation of SDEs

The SDEs parameter estimation problem is formulated as a maximum likelihood estimation (MLE) problem (Kristensen et al., 2004a). The maximum likelihood method is assumes the normality of the model residual. The states and the parameters $C_{0,i}$, $D^{'} = D_{(i-1,i),t}/\Delta x_m^2$, of the above formulated coupled SDEs are estimated from the dataset simulated using the PDE model described in Section 2.1. For the sequence of measurements $\mathcal{Z}_N$, the likelihood function can be formulated using the one-step prediction errors, $\epsilon_k = z_{t_k} - \hat{z}_{t_{k-1}}$, and the associated variances, $R_{t_k|t_{k-1}} = \mathrm{Var}(z_{t_k}|\mathcal{Z}_{t_{k-1}}, \theta)$ as below (Kristensen et al., 2004a):

$$\mathbb{L}(\theta; \mathcal{Z}_N) = p(\mathcal{Z}_N|\theta) \tag{19}$$

$$= \left(\prod_{k=1}^{N} \frac{\exp\left(-\frac{1}{2}\epsilon_{t_k}^T R_{t_k|t_{k-1}}^{-1}\epsilon_{t_k}\right)}{\sqrt{\det(R_{t_k|t_{k-1}})(\sqrt{2\pi})^{\mathcal{L}}}}\right)p(z_0|\theta)$$

where the set of parameters is represented by θ, the set of observations by $\mathcal{Z}_N$, the dimension of the observation space by $\mathcal{L}$, and z_0 is initial measurement. The parameter estimate is then obtained by minimising the negative log-likelihood:

$$\hat{\theta} = \underset{\theta\in\Theta}{\mathrm{argmin}}\{-\log(\mathbb{L}(\theta; \mathcal{Z}_N)|z_0)\}. \tag{20}$$

$$= -\frac{1}{2}\sum_{k=1}^{N}\Big(\epsilon_{t_k}^T R_{t_k|t_{k-1}}^{-1}\epsilon_{t_k} + \log\det R_{t_k|t_{k-1}}^{-1} \tag{21}$$

$$+ \mathcal{L}\log 2\pi\Big)$$

All computations were done using the free statistical software-R (version 3.3.2). and the "*CTSM-R-package*" (Continuous Time Stochastic Modelling in R version 0.6.8-5, (Juhl, 2015)).

5. RESULTS

This section describes the results obtained from the estimated SDE based model of the flow-front dynamics. For the estimation, the initial states are assumed to be known, and the boundary conditions of the PDE are not taken into account. This condition implies that the estimation data only included the time steps where the flow-front progression for all measurement lines is below 0.9 m. Furthermore, an additive noise of standard deviation 0.05 was added to the simulated flow-front data generated by the PDE solver before the estimation step.

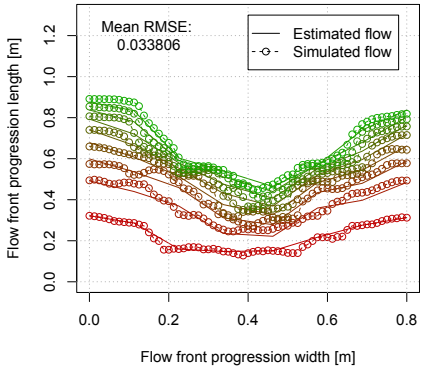

Fig. 5. Estimated heterogeneous flow after including the viscosity as an explicit state in SDE model.

Fig.5 and Fig.6 show the comparison of the estimated flow-front trajectories (solid lines) using the SDE model described in Section 4.1 and the simulated flow-front trajectories (dot-dashed) generated using the PDE model described in Section 2.1. Fig.5 show the estimated flow-front trajectory where both changes in permeability and

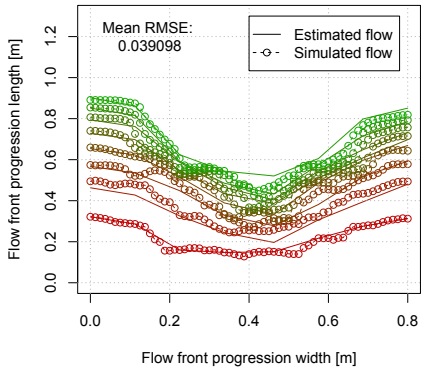

Fig. 6. Estimated heterogeneous flow where the viscosity is not included as an explicit state in SDE model.

viscosity are explicitly accounted for in the SDE model. The change in viscosity is captured by introducing it as a new dynamic state in the SDE model (see (17) and (18)). Whereas, Fig.6 shows an example of the estimated flow-front trajectory where the change in viscosity is not accounted for in the SDE model. It can be easily seen from Fig.6 the model without an extra dynamic state accounting for the change in viscosity underestimates the flow-front trajectories at most of the time steps due to the deficiency in the model structure. This is also validated by the mean root mean squared error (RMSE) of 0.033806 and 0.039098 between the simulated and the estimated flow-front trajectories where the dynamic viscosity state is included or not in the grey-box model respectively.

6. CONCLUSIONS AND FUTURE RESEARCH

A good understanding of the flow-front dynamics is essential for designing a monitoring system for controlling the epoxy flow inside the mould in a VARTM process. In this paper, we proposed a methodology to simulate the random changes in process parameters such as permeability and viscosity in a PDEs based model of the flow-front. Furthermore, a low-dimensional stochastic coupled SDEs based grey-box model of the flow-front dynamics is extended to accommodate such random changes in the process parameters. The proposed method has been validated on numerical simulation. Our future research aims to test the methodology for more complex flow patterns and to investigate its validity with real experimental data acquired using optical fibres and/or dielectric sensors.

REFERENCES

Alnæs, M.S., Blechta, J., Hake, J., Johansson, A., Kehlet, B., Logg, A., Richardson, C., Ring, J., Rognes, M.E., and Wells, G.N. (2015). The FEniCS project version 1.5. *Archive of Numerical Software*, 3(100).

Buchmann, C., Filsinger, J., and Ladstaetter, E. (2016). Investigation of electrical time domain reflectometry for infusion and cure monitoring in combination with electrically conductive fibers and tooling materials. *Composites Part B-engineering*, 94, 389–398. doi:10.1016/j.compositesb.2016.02.060.

Darcy, H. (1856). *Les fontaines publiques de la ville de Dijon: exposition et application ...* Victor Dalmont.

Dominauskas, A., Heider, D., and Gillespie, J.W. (2003). Electric time-domain reflectometry sensor for online flow sensing in liquid composite molding processing. *Composites Part A: Applied Science and Manufacturing*, 34(1), 67 – 74.

Juhl, R. (2015). *CTSM-R: Continuous Time Stochastic Modelling in R: User's Guide and Reference Manual*. R package version 0.6.8-5.

Kristensen, N.R., Madsen, H., and Jørgensen, S.B. (2004a). Parameter estimation in stochastic grey-box models. *Automatica*, 40(2), 225 – 237.

Kristensen, N.R., Madsen, H., and Jørgensen, S.B. (2004b). Stochastic grey-box modelling as a tool for improving the quality of first engineering principles models. *IFAC Proceedings Volumes*, 37(1), 143 – 148. 7th International Symposium on Advanced Control of Chemical Processes (ADCHEM 2003), Hong-Kong, 11-14 January 2004.

Kueh, S.R., Parnas, R.S., and Advani, S.G. (2002). A methodology for using long-period gratings and mold-filling simulations to minimize the intrusiveness of flow sensors in liquid composite molding. *Composites Science and Technology*, 62(2), 311 – 327.

Matsuzaki, R. and Shiota, M. (2016). Data assimilation through integration of stochastic resin flow simulation with visual observation during vacuum-assisted resin transfer molding: A numerical study. *Composites Part A: Applied Science and Manufacturing*, 84(Supplement C), 43 – 52.

Matuzaki, R., Seto, D., Naito, M., Todoroki, A., and Mizutani, Y. (2015). Analytical prediction of void formation in geometrically anisotropic woven fabrics during resin transfer molding. *Composites Science and Technology*, 107(Supplement C), 154 – 161.

Nauheimer, M., Relan, R., Thygesen, U.H., and Madsen, H. (2018a). Estimation of a stochastic spatio-temporal model of the flow-front dynamics with varying parameters. In *AIP Conference Proceedings*, volume 1981, 020098. AIP Publishing.

Nauheimer, M., Relan, R., Thygesen, U.H., Madsen, H., Olesen, B., and Kirkeby, K. (2018b). A stochastic spatio-temporal model of the flow-front dynamics in a vacuum assisted resin transfer moulding process. *IFAC-PapersOnLine*, 51(15), 383–388.

Øksendal, B. (2010). *Stochastic Differential Equations: An Introduction with Applications*. Universitext. Springer Berlin Heidelberg.

Park, C.H., Lebel, A., Saouab, A., Bréard, J., and Lee, W.I. (2011). Modeling and simulation of voids and saturation in liquid composite molding processes. *Composites Part A: Applied Science and Manufacturing*, 42(6), 658 – 668.

Stiesdal, H., Enevoldsen, P., Johansen, K., Kristensen, J., Nörtem, M., and Winther-Jensen, M. (2006). Method for manufacturing windmill blades. EP Patent 1,310,351.

Yenilmez, B. and Sozer, E.M. (2009). A grid of dielectric sensors to monitor mold filling and resin cure in resin transfer molding. *Composites Part A: Applied Science and Manufacturing*, 40(4), 476 – 489.

Zhang, F., Cosson, B., Comas-Cardona, S., and Binetruy, C. (2011). Efficient stochastic simulation approach for rtm process with random fibrous permeability. *Composites Science and Technology*, 71(12), 1478 – 1485.